

COVARIANCE REALISM IS NOT ENOUGH

J. Russell Carpenter*

A great deal of effort has been put into improving the practice of space situational awareness such that covariance data associated with predicted close approaches is more “realistic.” However, “realistic” usually has meant “larger” and this presents a problem. In many cases, there exist multiple sources for predictive ephemerides, which may be fused to produce predictive states with smaller associated covariances. Ancillary to the fusion computation is the capability to assess consistency of the estimates. If actionable covariance information becomes available, interval estimates for the miss distance provide a more informative alternative to collision probability for risk assessment.

INTRODUCTION

A great deal of effort has been put into improving the practice of space situational awareness (SSA) such that covariance data associated with predicted close approaches is more “realistic.” Reference 1 provides an comprehensive summary of such efforts to date. However, “realistic” usually has meant “larger” and this presents a problem. From the standpoint of an owner/operator who must decide what to do about a potentially hazardous close approach, if the covariance of the relative position near the likely interval of closest approach is too large, then the data available for making a decision are likely to produce a false alarm. These problems are exacerbated by the fact that the current standard for dissemination of covariance data permits the publication of defective covariances.

A long-standing concern with the covariances associated with the relative state between the primary and secondary objects, which are necessary for many conjunction assessment calculations, is that any non-zero cross-covariance between the solutions is ignored. As will be shown below, it is relatively easy to reconstruct such a cross-covariance, and there is good reason to believe that it is not zero (although in practice the resulting correction may be quite small).

In many cases, there exist multiple sources for predictive ephemerides, which may be fused to produce predictive states with smaller associated covariances. Unlike many applications of estimate fusion, the cross-covariance of the estimates to be fused is known. Ancillary to the fusion computation is the capability to assess consistency of the estimates. Covariance inflation factors may be explicitly computed to assess covariance realism. This paper contributes a description of aforementioned fusion techniques, and provides an example to illustrate their use in a hypothetical spacecraft conjunction.

*Deputy Project Manager/Technical, Space Science Mission Operations Project, NASA Goddard Space Flight Center, 8800 Greenbelt Rd, Greenbelt, MD 20771

If actionable covariance information becomes available, there remains the question of what to do with it. The current practice for most Earth orbiting missions is to use covariances to compute collision probabilities, but Reference 2 discusses some of shortcomings of this approach. This paper also describes how the same integrals used to compute collision probabilities may be used to compute interval estimates for the miss distance, expanding and clarifying the presentation in Reference 2, and illustrates the approach for a hypothetical conjunction.

COVARIANCE REPRESENTATION IN THE CONJUNCTION DATA MESSAGE

The current standard for exchanging conjunction information is the Conjunction Data Message (CDM), specified in a Consultative Committee for Space Data Systems Standard.³ As currently implemented, the CDM provides the lower triangular elements of the covariance matrix, in a radial, tangent, normal (RTN) coordinate frame. This can be problematic, because there is no guarantee that the covariance reconstructed from such a representation will be positive definite. Not infrequently, non-positive-definite (NPD) covariances do occur in operational usage of CDMs. Consideration of other representations seems warranted.

There are many alternatives for representing a covariance matrix that ensure positive definiteness, and some of these also increase numerical precision, in terms of, for example, condition number. Alternatives that retain the precision of the original covariance include singular-value/eigenvalue decompositions, and UDU^T (or LDL^T) factorizations. The UDU^T is a particularly efficient and compact representation and hence has been recommended as a best practice for navigation filtering.⁴ Alternatives that increase the precision are “square-root” factorizations, such as the Cholesky factorization. Not to be forgotten, if only for its readability, is a representation that utilizes standard deviations for its diagonal, and correlation coefficients for its off-diagonal elements; this method also increases numerical precision relative to a covariance representation. Unlike Cholesky however, the latter method does not require the original covariance to be strictly positive definite, or enforce that the reconstructed covariance will be positive either. Some of these alternatives may offer better interpolation properties as well. In any case, interpolation methods must be used with caution, particularly if they have the potential to introduce non-physical oscillations that can negatively affect the covariance eigenstructure.

Regardless of the representation chosen to avoid transmission of NPD covariances, additional consideration to the coordinatization is warranted. In addition to RTN, Reference 3 supports delivery of covariances in a tangent, velocity, normal (TVN) frame. The TVN frame would be expected to be superior to RTN for any orbit that is not perfectly circular, since its primary basis vector is the unit velocity vector, which is the direction of fastest growth when predicting covariances. If some SSA providers or owner/operators do not currently support delivery in the TVN frame, this should not be a sustainable justification for continuing to employ the inferior RTN representation.

CORRELATION BETWEEN PRIMARY AND SECONDARY OBJECT STATE ESTIMATES

The covariance corresponding to the relative state between two objects is given by

$$\mathbf{P}_{\text{rel}} = \mathbb{E} \left[(\mathbf{e}_1 - \mathbf{e}_2)(\mathbf{e}_1 - \mathbf{e}_2)^T \right] \quad (1)$$

$$= \mathbf{P}_1 + \mathbf{P}_2 - \mathbf{P}_{12} - \mathbf{P}_{12}^T \quad (2)$$

Usually, Conjunction Assessment (CA) applications assume that $\mathbf{P}_{12} = 0$. But suppose the Orbit Determination (OD) process for the two objects is estimating a common state, e.g. a density bias.

To see that $\mathbf{P}_{12} \neq 0$, consider the covariance of an estimate of all the states together.

Let α index the state unique to object 1, β the states unique to object 2, and γ the states common to both. Let the estimation error in the combined state be $\mathbf{e}_* = [\mathbf{e}_\alpha, \mathbf{e}_\beta, \mathbf{e}_\gamma]$, and let $\mathbf{e}_1 = [\mathbf{e}_\alpha, \mathbf{e}_\gamma]$ and $\mathbf{e}_2 = [\mathbf{e}_\beta, \mathbf{e}_\gamma]$ be the errors of individual object estimates. Then

$$\mathbf{e}_1 = \begin{bmatrix} \mathbf{I}_\alpha & \mathbf{0} & \mathbf{0} \\ \mathbf{0} & \mathbf{0} & \mathbf{I}_\gamma \end{bmatrix} \mathbf{e}_* = \mathbf{M}_1 \mathbf{e}_* \quad \text{and} \quad \mathbf{e}_2 = \begin{bmatrix} \mathbf{0} & \mathbf{I}_\beta & \mathbf{0} \\ \mathbf{0} & \mathbf{0} & \mathbf{I}_\gamma \end{bmatrix} \mathbf{e}_* = \mathbf{M}_2 \mathbf{e}_* \quad (3)$$

Let $\mathbf{P}_* = \mathbb{E}[\mathbf{e}_* \mathbf{e}_*^T]$. Then, \mathbf{P}_{12} will be given by

$$\mathbf{P}_{12} = \mathbf{M}_1 \mathbf{P}_* \mathbf{M}_2^T \quad (4)$$

$$= \begin{bmatrix} \mathbf{I}_\alpha & \mathbf{0} & \mathbf{0} \\ \mathbf{0} & \mathbf{0} & \mathbf{I}_\gamma \end{bmatrix} \begin{bmatrix} \mathbf{P}_{\alpha\alpha} & \mathbf{P}_{\alpha\beta} & \mathbf{P}_{\alpha\gamma} \\ \mathbf{P}_{\beta\alpha} & \mathbf{P}_{\beta\beta} & \mathbf{P}_{\beta\gamma} \\ \mathbf{P}_{\gamma\alpha} & \mathbf{P}_{\gamma\beta} & \mathbf{P}_{\gamma\gamma} \end{bmatrix} \begin{bmatrix} \mathbf{0} & \mathbf{0} \\ \mathbf{I}_\beta & \mathbf{0} \\ \mathbf{0} & \mathbf{I}_\gamma \end{bmatrix} \quad (5)$$

$$= \begin{bmatrix} \mathbf{P}_{\alpha\beta} & \mathbf{P}_{\alpha\gamma} \\ \mathbf{P}_{\gamma\beta} & \mathbf{P}_{\gamma\gamma} \end{bmatrix} \quad (6)$$

Even if the prior cross-covariances $\mathbf{P}_{\alpha\beta}$, $\mathbf{P}_{\alpha\gamma}$, and $\mathbf{P}_{\gamma\beta}$ are all zero, so long as the prior value of $\mathbf{P}_{\gamma\gamma} \neq 0$, then the posterior value of \mathbf{P}_{12} could be a full matrix. This is especially interesting because one might expect that the cross-covariance $\mathbf{P}_{\alpha\beta}$ would not be recoverable from two separate estimators, which do not share the α and β states in common.

In the context of separate batch least-squares orbit determination (BLSOD) processes for each of the objects, the computation of the cross-covariance could proceed as follows. Normally, the BLSOD differential correction at the anchor time, $\hat{\mathbf{x}}$, is cast in terms of a solution to the normal equation as follows, which may be (inefficiently) written

$$\hat{\mathbf{x}} = \left(\bar{\mathbf{P}}^{-1} + \tilde{\mathbf{H}}^T \mathbf{R}^{-1} \tilde{\mathbf{H}} \right)^{-1} \left(\bar{\mathbf{P}}^{-1} \bar{\mathbf{x}} + \tilde{\mathbf{H}}^T \mathbf{R}^{-1} \mathbf{y} \right) \quad (7)$$

where $\bar{\mathbf{P}}$ is assumed to approximate the prior covariance at the anchor time, $\bar{\mathbf{x}}$ is the associated prior correction (usually taken to be zero), $\tilde{\mathbf{H}}$ is the mapping of the measurement partials to the anchor time, \mathbf{R}^{-1} is the (usually diagonal) weighting matrix for the measurement innovations, and \mathbf{y} are the measurement innovations (differences between observed and computed measurements). The posterior covariance associated with the error in the differential correction is often approximated in BLSOD processes as $\hat{\mathbf{P}} = \left(\bar{\mathbf{P}}^{-1} + \tilde{\mathbf{H}}^T \mathbf{R}^{-1} \tilde{\mathbf{H}} \right)^{-1}$. Letting $\tilde{\mathbf{K}} = \hat{\mathbf{P}} \tilde{\mathbf{H}}^T \mathbf{R}^{-1}$, the posterior covariance may be algebraically manipulated into the following form:

$$\hat{\mathbf{P}} = \left(\mathbf{I} - \tilde{\mathbf{K}} \tilde{\mathbf{H}} \right) \bar{\mathbf{P}} \quad (8)$$

However, in either of these forms, $\hat{\mathbf{P}}$ will only represent the actual covariance if $\tilde{\mathbf{K}}$ is the optimal gain. If a suboptimal gain is used, it can be shown that the covariance is actually given by

$$\hat{\mathbf{P}} = \left(\mathbf{I} - \tilde{\mathbf{K}} \tilde{\mathbf{H}} \right) \bar{\mathbf{P}} \left(\mathbf{I} - \tilde{\mathbf{K}} \tilde{\mathbf{H}} \right)^T + \tilde{\mathbf{K}} \mathbf{R} \tilde{\mathbf{K}}^T \quad (9)$$

If the BLSOD process were estimating all of the states in one “full” vector, the cross-covariance $\mathbf{P}_{\alpha\beta}$ would be present as a partition of the full covariance, $\hat{\mathbf{P}}_*$ given by one of the forms above.

Since the individual BLSOD processes only estimate their own states, then $\hat{\mathbf{P}}_1$ and $\hat{\mathbf{P}}_2$, and the corresponding gain matrices $\tilde{\mathbf{K}}_1$ and $\tilde{\mathbf{K}}_2$, will be missing some terms containing $\mathbf{P}_{\alpha\beta}$, as well as products of cross-covariances they do contain with the weighting matrices of the measurements on the other object they do not process. For this reason, such estimators are suboptimal. Nonetheless, so long as they are both estimating some common states, then as described above, a non-zero posterior cross-covariance may arise. Assuming both estimators use the same prior covariance for the common states, this approximate posterior cross-covariance will be given by

$$\hat{\mathbf{P}}_{12} = \left(\mathbf{I} - \tilde{\mathbf{K}}_1 \tilde{\mathbf{H}}_1 \right) \bar{\mathbf{P}}_{12} \left(\mathbf{I} - \tilde{\mathbf{K}}_2 \tilde{\mathbf{H}}_2 \right)^\top \quad (10)$$

$$= \hat{\mathbf{P}}_1 \bar{\mathbf{P}}_1^{-1} \bar{\mathbf{P}}_{12} \bar{\mathbf{P}}_2^{-1} \hat{\mathbf{P}}_2 \quad (11)$$

$$= \begin{bmatrix} \hat{\mathbf{P}}_{1\alpha\alpha} & \hat{\mathbf{P}}_{1\alpha\gamma} \\ \hat{\mathbf{P}}_{1\gamma\alpha} & \hat{\mathbf{P}}_{1\gamma\gamma} \end{bmatrix} \begin{bmatrix} \bar{\mathbf{P}}_{\alpha\alpha}^{-1} & \mathbf{0} \\ \mathbf{0} & \bar{\mathbf{P}}_{\gamma\gamma}^{-1} \end{bmatrix} \begin{bmatrix} \mathbf{0} & \mathbf{0} \\ \mathbf{0} & \bar{\mathbf{P}}_{\gamma\gamma} \end{bmatrix} \begin{bmatrix} \bar{\mathbf{P}}_{\beta\beta}^{-1} & \mathbf{0} \\ \mathbf{0} & \bar{\mathbf{P}}_{\gamma\gamma}^{-1} \end{bmatrix} \begin{bmatrix} \hat{\mathbf{P}}_{2\beta\beta} & \hat{\mathbf{P}}_{2\beta\gamma} \\ \hat{\mathbf{P}}_{2\gamma\beta} & \hat{\mathbf{P}}_{2\gamma\gamma} \end{bmatrix} \quad (12)$$

$$= \begin{bmatrix} \hat{\mathbf{P}}_{1\alpha\gamma} \bar{\mathbf{P}}_{\gamma\gamma}^{-1} \hat{\mathbf{P}}_{2\beta\gamma}^\top & \hat{\mathbf{P}}_{1\alpha\gamma} \bar{\mathbf{P}}_{\gamma\gamma}^{-1} \hat{\mathbf{P}}_{2\gamma\gamma} \\ \hat{\mathbf{P}}_{1\gamma\gamma} \bar{\mathbf{P}}_{\gamma\gamma}^{-1} \hat{\mathbf{P}}_{2\beta\gamma}^\top & \hat{\mathbf{P}}_{1\gamma\gamma} \bar{\mathbf{P}}_{\gamma\gamma}^{-1} \hat{\mathbf{P}}_{2\gamma\gamma} \end{bmatrix} \quad (13)$$

Note that this result is unchanged if either or both $\bar{\mathbf{P}}_{\alpha\alpha}^{-1} = \mathbf{0}$ or $\bar{\mathbf{P}}_{\beta\beta}^{-1} = \mathbf{0}$. In practice, so long as $\bar{\mathbf{P}}_{\gamma\gamma}$ is large relative to $\hat{\mathbf{P}}_{1\gamma\gamma}$ and $\hat{\mathbf{P}}_{2\gamma\gamma}$, then subtraction of $\hat{\mathbf{P}}_{12}$ and its transpose from the sum of $\hat{\mathbf{P}}_1$ and $\hat{\mathbf{P}}_2$ will be a small correction to \mathbf{P}_{rel} .

As an illustrative example, consider the following ‘‘one-dimensional’’ case:

$$\begin{aligned} \hat{\mathbf{P}}_1 &= \begin{bmatrix} \hat{\mathbf{P}}_{1\alpha\alpha} & \hat{\mathbf{P}}_{1\alpha\gamma} \\ \hat{\mathbf{P}}_{1\gamma\alpha} & \hat{\mathbf{P}}_{1\gamma\gamma} \end{bmatrix} = \begin{bmatrix} 1 \times 10^8 & 50 \\ 50 & 1 \times 10^{-4} \end{bmatrix}, \\ \hat{\mathbf{P}}_2 &= \begin{bmatrix} \hat{\mathbf{P}}_{2\beta\beta} & \hat{\mathbf{P}}_{2\beta\gamma} \\ \hat{\mathbf{P}}_{2\gamma\beta} & \hat{\mathbf{P}}_{2\gamma\gamma} \end{bmatrix} = \begin{bmatrix} 2.5 \times 10^7 & 12.5 \\ 12.5 & 2.5 \times 10^{-5} \end{bmatrix} \\ \hat{\mathbf{P}}_1 + \hat{\mathbf{P}}_2 &= \begin{bmatrix} 1.25 \times 10^8 & 62.5 \\ 62.5 & 1.25 \times 10^{-4} \end{bmatrix} \end{aligned} \quad (14)$$

Suppose $\bar{\mathbf{P}}_{\gamma\gamma} = 100$. Then

$$\hat{\mathbf{P}}_{12} = \begin{bmatrix} 6.25 & 12.5 \\ 12.5 & 2.5 \times 10^{-11} \end{bmatrix}$$

and

$$\hat{\mathbf{P}}_1 + \hat{\mathbf{P}}_2 - \hat{\mathbf{P}}_{12} - \hat{\mathbf{P}}_{12}^\top = \begin{bmatrix} 1.249999875 \times 10^8 & 62.499975 \\ 62.499975 & 1.2499995 \times 10^{-4} \end{bmatrix}$$

which is a negligible change from Eq. (14). Suppose $\bar{\mathbf{P}}_{\gamma\gamma} = 1 \times 10^{-4}$. Then

$$\hat{\mathbf{P}}_{12} = \begin{bmatrix} 6.25 \times 10^6 & 12.5 \times 10^{-6} \\ 12.5 \times 10^{-6} & 2.5 \times 10^{-5} \end{bmatrix}$$

and

$$\hat{\mathbf{P}}_1 + \hat{\mathbf{P}}_2 - \hat{\mathbf{P}}_{12} - \hat{\mathbf{P}}_{12}^\top = \begin{bmatrix} 1.125 \times 10^8 & 37.5 \\ 37.5 & 7.5 \times 10^{-5} \end{bmatrix}$$

which is a notable change from Eq. (14).

In practice, the large $\bar{\mathbf{P}}_{\gamma\gamma}$ scenario illustrated by the first subcase above is likely far more typical than a small $\bar{\mathbf{P}}_{\gamma\gamma}$ scenario. Nonetheless, given the simplicity of the above computation, SSA providers employing BLSOD should communicate any common *a priori* covariance values used to constrain both primary and secondary object solutions, so that owner/operators have the option to include a cross-covariance in their computations of \mathbf{P}_{rel} . SSA providers employing sequential filtering methods that simultaneously estimate both objects in one state vector can merely supply the full covariance, from which the cross-covariance can be extracted*. Adopting such practices would also comply with ASA Principle 4 “Proper inference requires full reporting and transparency.”²

FUSION

Bar-Shalom described fusion in terms of a measurement innovation that is the difference between two Kalman filters’ posterior estimates of a common state.^{5,6,7,8} This work was generalized by Carpenter and Bishop,⁹ who developed a posterior estimate fusion approach that optimally utilizes cross-covariances between common and non-common states within and between the two estimators. Julier and Uhlmann formulated an alternative¹⁰ known as *covariance intersection* that does not require knowledge of cross-covariances; for reasons discussed below, this method is not applicable nor desirable in the present case.

Let \mathbf{a} denote a random vector whose realization is the true state for one of the estimators, and \mathbf{b} the state of the other. Let ξ denote the states common to both estimators, η the states unique to estimator whose state is \mathbf{a} , and ζ the states unique to estimator whose state is \mathbf{b} . Ref. 9 shows that assuming a linear, unbiased fusion of the common states,

$$\hat{\mathbf{c}}_{\xi} = (\mathbf{I} - \mathbf{W})\hat{\mathbf{a}}_{\xi} + \mathbf{W}\hat{\mathbf{b}}_{\xi} \quad (15)$$

and choosing the gain matrix, \mathbf{W} , to minimize the trace of \mathbf{P}_c , results in

$$\mathbf{W}_* = (\mathbf{P}_{a\xi\xi} - \mathbf{P}_{ab\xi\xi})(\mathbf{P}_{a\xi\xi} + \mathbf{P}_{b\xi\xi} - \mathbf{P}_{ab\xi\xi} - \mathbf{P}_{ab\xi\xi}^{\text{T}})^{-1} \quad (16)$$

Using the optimal gain, the various partitions of \mathbf{P}_c become

$$\mathbf{P}_{c\xi\xi} = \mathbf{P}_{a\xi\xi} - \mathbf{W}_*(\mathbf{P}_{a\xi\xi} - \mathbf{P}_{ab\xi\xi}^{\text{T}}) \quad (17)$$

$$\mathbf{P}_{c\xi\eta} = \mathbf{P}_{a\xi\eta} - \mathbf{W}_*(\mathbf{P}_{a\xi\eta} - \mathbf{P}_{ab\xi\eta}^{\text{T}}) \quad (18)$$

$$\mathbf{P}_{c\xi\zeta} = \mathbf{P}_{ab\xi\zeta} - \mathbf{W}_*(\mathbf{P}_{ab\xi\zeta} - \mathbf{P}_{b\xi\zeta}^{\text{T}}) \quad (19)$$

$$\mathbf{P}_{c\eta\eta} = \mathbf{P}_{a\eta\eta}, \quad \mathbf{P}_{c\zeta\zeta} = \mathbf{P}_{b\zeta\zeta}, \quad \mathbf{P}_{c\eta\zeta} = \mathbf{P}_{ab\eta\zeta} \quad (20)$$

Noting that fusion gain given by Eq. (16) contains the covariance of the difference between the common states of the two estimators $\mathbf{d} = \mathbf{a}_{\xi} - \mathbf{b}_{\xi}$,

$$\mathbb{E}\left[(\mathbf{a}_{\xi} - \mathbf{b}_{\xi})(\mathbf{a}_{\xi} - \mathbf{b}_{\xi})^{\text{T}}\right] = \mathbf{P}_d = \mathbf{P}_{a\xi\xi} + \mathbf{P}_{b\xi\xi} - \mathbf{P}_{ab\xi\xi} - \mathbf{P}_{ab\xi\xi}^{\text{T}} \quad (21)$$

a test for consistency between the estimates may be readily performed using a χ^2 statistic

$$k_d^2 = \mathbf{d}^{\text{T}}\mathbf{P}_d^{-1}\mathbf{d} \quad (22)$$

If a consistency threshold is exceeded, i.e. $k_d^2 > \chi_{1-\alpha}^2$, covariance realism may be in doubt, and the ratio $r = k_d^2/\chi_{1-\alpha}^2$ may be used to inflate the constituent covariances to $r\mathbf{P}_{a\xi\xi}$, $r\mathbf{P}_{b\xi\xi}$, and $r\mathbf{P}_{ab\xi\xi}$.

*Providing a full covariance for both objects simultaneously via the existing CDM mechanism would require a revision to Reference 3

Application to Conjunction Assessment

In a typical operational context, conjunction data messages (CDM) containing predictive states and covariances for both objects are available from a space situational awareness (SSA) data provider, such as the United States Department of Defense Combined Space Operations Center. In many cases, one or both of the objects will also have conjunction data products available from its owner/operator (O/O). Table 1 summarizes the permutations of states potentially available for fusion. The partition

Table 1: Fusion Permutations.

State a Source		State b Source		Absolute Fusion States	Relative Cross-Covariance States
Primary	Secondary	Primary	Secondary		
O/O	SSA	SSA	SSA	Primary	Secondary
SSA	SSA	O/O	SSA	Primary	Secondary
O/O	O/O	SSA	O/O	Primary	Secondary
SSA	O/O	O/O	O/O	Primary	Secondary
SSA	O/O	SSA	SSA	Secondary	Primary
SSA	SSA	SSA	O/O	Secondary	Primary
O/O	O/O	O/O	SSA	Secondary	Primary
O/O	SSA	O/O	O/O	Secondary	Primary
O/O	O/O	SSA	SSA	Both	None
SSA	SSA	O/O	O/O	Both	None

of common states, ξ , to be fused according to Eq. (15) will include at least the position and velocity of one of the two objects, and may also include some common parameters, e.g. related to ballistic modeling.

Fusion of the absolute states of either the primary, the secondary, or both object(s) may be performed, according the penultimate column of Table 1. The rows paired within horizontal rules are similar conjunction assessments, i.e. the first two rows both result in fusion of the state of the primary object for comparison with the SSA provider’s estimate of the secondary object. In the case of such absolute state fusion, the cross-covariance \mathbf{P}_{ab} may safely be assumed to be zero.*

Alternatively, the two object states may be differenced to produce a relative state, and their co-

*The relevant cross-covariance in this context must be the formal cross-covariance of the two estimators, i.e. the cross-covariance arising from shared modeling assumptions, such as common *a priori* covariance, common process noise, or common measurement noise. There are two conditions that could violate this assumption, both of which appear to be relatively unlikely, at least in the present operational paradigm: (1) the O/O and SSA provider are using common measurements in their orbit determination process, and/or (2) the O/O and the SSA provider are using the same astrodynamics software with the same settings. Any “true” or empirical cross-covariance arising from common mis-modeling by the two estimators is not relevant to the fusion gain calculation, and if it were to be used would not guarantee the invertibility of \mathbf{P}_d .

variances summed to produce a relative covariance.*

$$\widehat{\mathbf{a}}_r = \widehat{\mathbf{a}}_2 - \widehat{\mathbf{a}}_1, \quad \mathbf{P}_{ar} = \mathbf{P}_{a2} + \mathbf{P}_{a1} \quad (23)$$

$$\widehat{\mathbf{b}}_r = \widehat{\mathbf{b}}_2 - \widehat{\mathbf{b}}_1, \quad \mathbf{P}_{br} = \mathbf{P}_{b2} + \mathbf{P}_{b1} \quad (24)$$

$$(25)$$

where the subscripts 1 and 2 denote the primary and secondary object, respectively; as with absolute fusion, the differences may include not only position and velocity, but may also include applicable parameters. If the relative states are fused, then the object in the relative combination whose state derives from a common source will correlate the estimates. Hence, the cross-covariance \mathbf{P}_{ab} between the estimators must be equal to the absolute covariance of the object common to both relative state solutions, as shown in the final column of Table 1, assuming the source provider's estimates of the objects are uncorrelated. For example, considering the first row of Table 1, $\widehat{\mathbf{b}}_2 = \widehat{\mathbf{a}}_2$ as both are the same SSA provider estimate of the secondary object, and thus

$$\mathbf{P}_{ab} = \mathbb{E}[(\mathbf{a}_2 - \mathbf{a}_1)(\mathbf{a}_2 - \mathbf{b}_1)^\top] = \mathbf{P}_{a2} = \mathbf{P}_{b2} \quad (26)$$

Note that Eq. (26) implies that $\mathbf{P}_{ab\xi\xi} = \mathbf{P}_{a\xi\xi}$, $\mathbf{P}_{ab\xi\eta} = \mathbf{P}_{a\xi\eta}$ and $\mathbf{P}_{ab\xi\zeta} = \mathbf{P}_{b\xi\zeta}^\top$, which in turn implies from Eqs. (18) and (19) that $\mathbf{P}_{c\xi\eta} = \mathbf{P}_{a\xi\eta}$ and $\mathbf{P}_{c\xi\zeta} = \mathbf{P}_{b\xi\zeta}^\top$. Thus, only Eq. (17) need be computed in the present context. Note also that for the last two rows of Table 1, $\mathbf{P}_{ab} = 0$, since there are no common absolute state estimates.

In practice the CDM associated with $\widehat{\mathbf{a}}$ and $\widehat{\mathbf{b}}$ may have small differences in their predicted times of closest approach (TCA). While mapping the states and covariances to a common TCA can be performed with either absolute or relative states, relative state fusion may be preferable, since simpler approximations for the mapping may be applicable. In particular, if the short encounter assumptions^{11,12} for the conjunction hold, velocity uncertainty may be neglected, and only the relative position vector and its error covariance at TCA are needed. The mapping of the state and covariance associated with \mathbf{b} from \hat{t}_b to \hat{t}_a thus becomes

$$\widehat{\mathbf{b}}_r(\hat{t}_a) = \widehat{\mathbf{b}}_r(\hat{t}_b) \quad (27)$$

$$\mathbf{P}_{br}(\hat{t}_a) = \mathbf{P}_{br}(\hat{t}_b) \quad (28)$$

where \hat{t}_i , $i \in \{a, b\}$ denotes the TCA associated with $\widehat{\mathbf{a}}$ and $\widehat{\mathbf{b}}$, respectively.

When velocity uncertainty cannot be ignored,^{13,14} the full state and covariance must be mapped using an appropriate state transition matrix, $\Phi(\hat{t}_a, \hat{t}_b)$. In such cases, the relative cross-covariance requires some additional manipulation when $\widehat{\mathbf{a}}$ and $\widehat{\mathbf{b}}$ are not contemporaneous. Factorization of \mathbf{P}_{ab} facilitates mapping of the factor arising from $\widehat{\mathbf{b}}$ separately from the factor due to $\widehat{\mathbf{a}}$. Again with reference to the first row of Table 1 for specificity, such a factorization becomes

$$\mathbf{P}_{ab}(\hat{t}_a) = \mathbb{E}[\{\mathbf{a}_2(\hat{t}_a) - \mathbf{a}_1(\hat{t}_a)\} \{\mathbf{b}_2(\hat{t}_b) - \mathbf{b}_1(\hat{t}_b)\}^\top \Phi^\top(\hat{t}_a, \hat{t}_b)] \quad (29)$$

$$= \sqrt[3]{\mathbf{P}_{a2}(\hat{t}_a)} \left[\sqrt[3]{\Phi(\hat{t}_a, \hat{t}_b) \mathbf{P}_{b2}(\hat{t}_b) \Phi^\top(\hat{t}_a, \hat{t}_b)} \right]^\top \quad (30)$$

*For a given estimator, the cross-covariance between primary and secondary object states is typically assumed to be zero, although use of common modeling within the same estimator for both objects, e.g. for ballistic properties, may invalidate this assumption, as discussed in the previous section.

where $\sqrt{\cdot}$ indicates the Cholesky factor of the matrix under the radical, with the convention that $\mathbf{A} = \sqrt{\mathbf{A}} \left[\sqrt{\mathbf{A}} \right]^T$.

Fusion Example

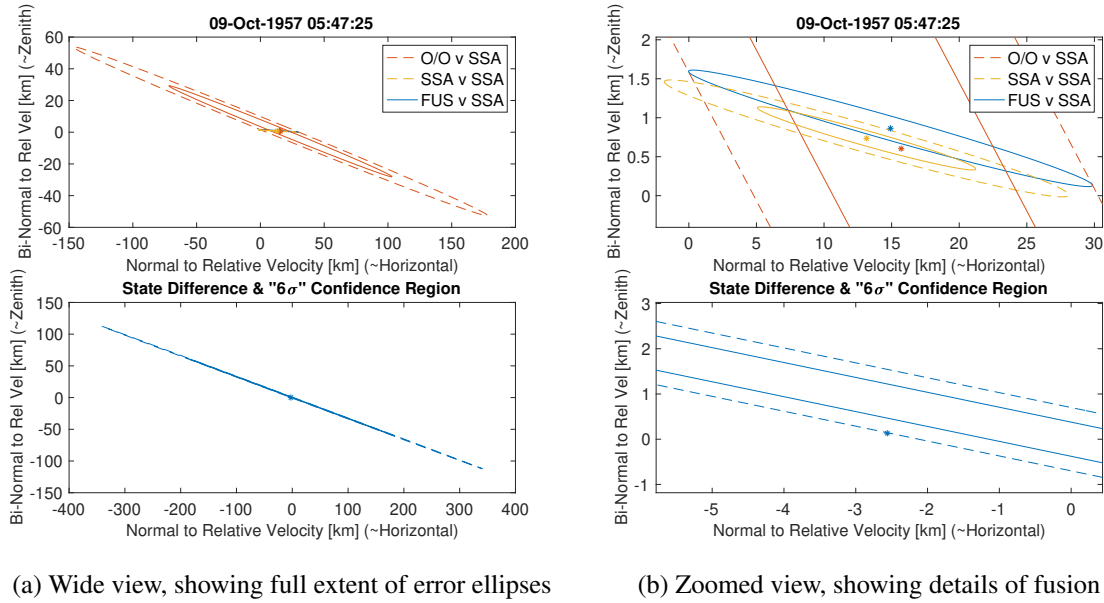


Figure 1: Confidence regions for fusion example. The upper plots show 3σ error ellipses centered on estimates indicated by asterisks. The lower plots show the difference between the estimates as an asterisk, and its associated “ 6σ ” confidence region. Dashed lines indicate covariances that have been inflated.

To illustrate the techniques this paper describes, this section utilizes an hypothetical close approach between two space objects satisfying the aforementioned short encounter assumptions. For such conjunctions, the relative position uncertainty near the nominal time of closest approach projects entirely into a plane normal to the relative velocity vector, known as the conjunction plane. The upper panels of Figure 1 illustrate the 3σ confidence regions projected into the conjunction plane for the example. Under the short encounter assumptions, these confidence regions (CR) are ellipses derived from the estimators’ covariance matrices, centered on the state estimates. For this example, the O/O estimate has a large CR in comparison to the CR of the SSA provider. Because the estimates are tightly grouped in comparison to the size of the error ellipses, one may observe that a zero-mean error ellipse associated with the fusion of the estimates would lie within the intersection of the zero-mean error ellipses from the the two estimators undergoing fusion, as had been observed by Carpenter and Bishop.¹⁵

The dashed ellipses in Figure 1 indicate covariances that have been inflated in order to satisfy a “ 6σ ” consistency test per Eq. (22). What is meant by “ 6σ ” is a probability threshold of 0.999999998, which corresponds to 6σ for a scalar Gaussian, but must correspond to a χ ratio of 6.33 for the conjunction plane projection, which has 2 degrees of freedom, or 6.59 if three degrees of freedom are considered. The original unscaled ellipses are plotted with solid lines of the same color. The lower panels of Figure 1 show the difference between the estimates, also projected into the conjunction

plane, and its corresponding “ 6σ ” ellipse. Note in Figure 1(b) that the difference lies outside its “ 6σ ” unscaled ellipse, plotted with a solid line, indicating an inconsistency between the estimates and a need for inflation. This inconsistency is not obvious in the upper panel of Figure 1(b), where the estimates appear to lie within each others’ 3σ error ellipses, since these ellipses do not account for the correlation between the estimates captured by \mathbf{P}_{ab} .

An interesting feature of the fusion in this case is how it accommodates the large difference between the size of the O/O-based estimate and the SSA-only estimate, and the strong correlations present in each. A fusion which ignored the correlation structure associated with each estimate would place the fused estimate on a line connecting the two estimates being fused, with the placement of the fused estimate along that line dependent on the relative uncertainty between the estimates being fused. The upper panel of Figure 1(b) shows that the optimal fusion preferentially offsets the fused estimate along the major axis of the more uncertain estimate, folding its strong correlation structure into the fusion so as to follow a sort of probabilistic geodesic. To the extent that the correlation structure among all the parameters being fused is dominated by the correlations within the individual estimates, and not the correlations between the estimates modeled by \mathbf{P}_{ab} , the covariance intersection method can also follow such geodesics. When the opposite is true, covariance intersection cannot follow such geodesics, since it ignores the presence of \mathbf{P}_{ab} . While this may seem like a minor point, note that the differences among the three estimates in Figure 1(b) are all much greater than the typical combined hard-body involved in a conjunction.

DISTRIBUTION AND DENSITY FUNCTIONS FOR THE MISS DISTANCE

Many conjunctions occur over very short time intervals, allowing relative velocity uncertainty to be neglected. In such cases, the relative position uncertainty near the nominal time of closest approach projects entirely into a plane normal to the relative velocity vector, known as the conjunction plane. Various computations of P_c integrate this planar uncertainty over a disk in the plane corresponding to the combined hard-body radii (HBR) of the two conjuncting objects. When the state uncertainties follow a Gaussian distribution, P_c calculations using quadratures of relatively simple integrals are possible. When the short encounter assumptions cannot be satisfied, but the assumption of Gaussian errors remains valid, Coppola’s expression for collision probability¹³ may be employed.

Short Encounter Case

The cumulative probability that the relative position vector, \vec{R}_i , predicted from time t_i , is within a region defined by a set \mathcal{D}_r , which defines a circular disk in the conjunction plane and centered on

the origin, where the miss distance is less than or equal to some specified value r , is given by

$$F_{R_i}(r | \vec{\mu}_{\vec{R}}, P_{\vec{R}\vec{R}_i}) = \Pr(R_i \leq r) \quad (31)$$

$$= \frac{1}{\sqrt{|2\pi P_{\vec{R}\vec{R}_i}|}} \int_{\vec{X} \in \mathcal{D}_r} e^{-\frac{1}{2}(\vec{X} - \vec{\mu}_{\vec{R}})^T P_{\vec{R}\vec{R}_i}^{-1} (\vec{X} - \vec{\mu}_{\vec{R}})} d^2 \vec{X} \quad (32)$$

$$= \frac{1}{\sqrt{8\pi\sigma_{ib}}} \int_{-r}^r \exp\left(-\frac{(\mu_b + X_b)^2}{2\sigma_{ib}^2}\right) \times \left\{ \operatorname{erf}\left(\frac{\mu_a + \sqrt{r^2 - X_b^2}}{\sqrt{2}\sigma_{ia}}\right) - \operatorname{erf}\left(\frac{\mu_a - \sqrt{r^2 - X_b^2}}{\sqrt{2}\sigma_{ia}}\right) \right\} dX_b \quad (33)$$

$$= \int_{-r}^r \phi_2(X_b, r | \vec{\mu}_{\vec{R}}, P_{\vec{R}\vec{R}_i}) dX_b \quad (34)$$

where $R_i = \|\vec{R}_i\|$, and Eq. (33) follows from Afriend¹⁶ and Alfano.¹⁷ In Eq. (33), a and b denote the major and minor axes of the ellipse associated with the relative position covariance $P_{\vec{R}\vec{R}_i}$ projected into the conjunction plane, σ_{ia}^2 and σ_{ib}^2 are the associated eigenvalues of $P_{\vec{R}\vec{R}_i}$, μ_a and μ_b are the coordinates of $\vec{\mu}_{\vec{R}}$ along the corresponding conjunction plane axes, and the variable of integration, X_b , is the coordinate of the vector of integration \vec{X} , in Eq. (32), along the minor axis.

Noting that $\phi_2(r, r | \vec{\mu}_{\vec{R}}, P_{\vec{R}\vec{R}_i}) = \phi_2(-r, r | \vec{\mu}_{\vec{R}}, P_{\vec{R}\vec{R}_i}) = 0$, the associated probability density is given by

$$f_{R_i}(r | \vec{\mu}_{\vec{R}}, P_{\vec{R}\vec{R}_i}) = \Pr(r \leq R_i \leq r + dr) \quad (35)$$

$$= \frac{\partial}{\partial r} \int_{-r}^r \phi_2(X_b, r | \vec{\mu}_{\vec{R}}, P_{\vec{R}\vec{R}_i}) dX_b \quad (36)$$

$$= \phi_2(r, r | \vec{\mu}_{\vec{R}}, P_{\vec{R}\vec{R}_i}) + \phi_2(-r, r | \vec{\mu}_{\vec{R}}, P_{\vec{R}\vec{R}_i}) + \int_{-r}^r \phi_2'(X_b, r | \vec{\mu}_{\vec{R}}, P_{\vec{R}\vec{R}_i}) dX_b \quad (37)$$

$$= \int_{-r}^r \phi_2'(X_b, r | \vec{\mu}_{\vec{R}}, P_{\vec{R}\vec{R}_i}) dX_b \quad (38)$$

$$= \frac{1}{\sqrt{8\pi\sigma_{ib}}} \int_{-r}^r \frac{2r}{\sigma_{ia}\sqrt{2\pi(r^2 - X_b^2)}} \exp\left(-\frac{(X_b + \mu_b)^2}{2\sigma_{ib}^2}\right) \times \left\{ \exp\left(-\frac{[\mu_a + \sqrt{r^2 - X_b^2}]^2}{2\sigma_{ia}^2}\right) + \exp\left(-\frac{[\mu_a - \sqrt{r^2 - X_b^2}]^2}{2\sigma_{ia}^2}\right) \right\} dX_b \quad (39)$$

Case Including Velocity Uncertainty

Coppola¹³ breaks the computation including velocity uncertainty into two integrals: an integral over the combined hard-body volume at an initial time, and an integral over the time of the encounter, and over the surface of the hard-body volume. By choosing the initial time sufficiently in advance of the time of closest approach, it is often possible to consider only the latter integral. In such cases, the cumulative probability that the relative position vector, \vec{R}_i , predicted from time t_i , is

within a region defined by a set \mathcal{S}_r , which defines a spherical volume centered on the origin, where the miss distance is less than or equal to some specified value r , is given by

$$F_{Ri}(r | \vec{\mu}, P_i) = \Pr (R_i \leq r) \quad (40)$$

$$= \frac{1}{\sqrt{|2\pi P_{\vec{R}\vec{R}i}|}} \int_{t_o}^{t_o+T} \int_0^{2\pi} \int_{-\frac{\pi}{2}}^{\frac{\pi}{2}} e^{-\frac{1}{2}(\vec{R}_i - \vec{\mu}_{\vec{R}})^\top P_{\vec{R}\vec{R}i}^{-1}(\vec{R}_i - \vec{\mu}_{\vec{R}})} \nu(\vec{R}_i, t) r^2 \cos \theta \, d\theta \, d\phi \, dt \quad (41)$$

$$= \int_{t_o}^{t_o+T} \int_0^{2\pi} \int_{-\frac{\pi}{2}}^{\frac{\pi}{2}} \mathcal{N}_3(\vec{R}_i, \vec{\mu}_{\vec{R}}, P_{\vec{R}\vec{R}i}) \nu(\vec{R}_i, t) r^2 \cos \theta \, d\theta \, d\phi \, dt \quad (42)$$

$$= \int_{t_o}^{t_o+T} \int_0^{2\pi} \int_{-\frac{\pi}{2}}^{\frac{\pi}{2}} \phi_4(r, t, \theta, \phi | \vec{\mu}, P_i) \cos \theta \, d\theta \, d\phi \, dt \quad (43)$$

where

$$\nu(\vec{R}_i, t) = \frac{\sigma(\vec{R}_i, t)}{\sqrt{2\pi}} \exp\left(-\frac{\nu_o^2(\vec{R}_i, t)}{\sigma^2(\vec{R}_i, t)}\right) - \frac{\nu_o(\vec{R}_i, t)}{2} \left[1 - \operatorname{erf}\left(\frac{\nu_o(\vec{R}_i, t)}{\sigma(\vec{R}_i, t)\sqrt{2}}\right)\right] \quad (44)$$

$$\nu_o(\vec{R}_i, t) = \vec{u}_{\vec{R}i}^\top \left[\vec{\mu}_{\vec{V}} + P_{\vec{R}\vec{V}i} P_{\vec{R}\vec{R}i}^{-1} (R_i \vec{u}_{\vec{R}i} - \vec{\mu}_{\vec{R}}) \right] \quad (45)$$

and

$$\sigma(\vec{R}_i, t) = \vec{u}_{\vec{R}i}^\top \left(P_{\vec{V}\vec{V}i} - P_{\vec{R}\vec{V}i} P_{\vec{R}\vec{R}i}^{-1} P_{\vec{R}\vec{V}i}^\top \right) \vec{u}_{\vec{R}i} \quad (46)$$

Coppola points out that Eq. (41) may be efficiently evaluated using a Lebedev quadrature over the surface \mathcal{S}_r and a one-dimensional quadrature over the encounter time.

Since the limits of integration of Eq. (41) do not involve r , the associated PDF is

$$f_{Ri}(r | \vec{\mu}_{\vec{R}}, P_{\vec{R}\vec{R}i}) = \Pr (r \leq R_i \leq r + dr) \quad (47)$$

$$= \int_{t_o}^{t_o+T} \int_0^{2\pi} \int_{-\frac{\pi}{2}}^{\frac{\pi}{2}} \phi_4'(r, t, \theta, \phi | \vec{\mu}, P_i) \cos \theta \, d\theta \, d\phi \, dt \quad (48)$$

$$= \int_{t_o}^{t_o+T} \int_0^{2\pi} \int_{-\frac{\pi}{2}}^{\frac{\pi}{2}} \mathcal{N}_3(\vec{R}_i, \vec{\mu}_{\vec{R}}, P_{\vec{R}\vec{R}i}) \left[\frac{2\nu(\vec{R}_i, t)}{r} - (\vec{R}_i - \vec{\mu}_{\vec{R}})^\top P_{\vec{R}\vec{R}i}^{-1} \vec{u}_{\vec{R}i} \nu(\vec{R}_i, t) + \frac{\partial \nu(\vec{R}_i, t)}{\partial r} \right] r^2 \cos \theta \, d\theta \, d\phi \, dt \quad (49)$$

where

$$\frac{\partial \nu(\vec{R}_i, t)}{\partial r} = \left\{ \frac{\nu_o(\vec{R}_i, t)}{\sigma(\vec{R}_i, t)\sqrt{2\pi}} \exp\left(-\frac{\nu_o^2(\vec{R}_i, t)}{\sigma^2(\vec{R}_i, t)}\right) - \frac{1}{2} \left[1 - \operatorname{erf}\left(\frac{\nu_o(\vec{R}_i, t)}{\sigma(\vec{R}_i, t)\sqrt{2}}\right)\right] \right\} \vec{u}_{\vec{R}i}^\top P_{\vec{R}\vec{V}i} P_{\vec{R}\vec{R}i}^{-1} \vec{u}_{\vec{R}i} \quad (50)$$

which may similarly be evaluated using Lebedev quadrature over the surface and a one-dimensional quadrature over the encounter time.

MISS DISTANCE INTERVAL ESTIMATES

A common practice in conjunction assessment is to evaluate integrals such as Eq. (33) or Eq. (41) with $r = r_{HBR}$, where r_{HBR} denotes the combined hard-body radius of the participants in the conjunction. The resulting quantity, typically denoted P_c , is associated with the probability that the objects will collide. In mission operations, the parameters (mean and covariance) of the distributions are unknown, and hence operators must use estimates derived from tracking data. In the absence of prior distributions for the parameters (or the unwillingness to assume them), and assuming the parameters are not modeled as stochastic quantities, the only uncertainty associated with the parameter estimates arises from errors in the tracking data. As of this writing, it is the author's perception that such assumptions are broadly typical of current operational practices.

It is notable that under such assumptions, at the the time an operator predicts the latest state estimate and covariance to the time of closest approach, any errors in the tracking data have already been realized. These realizations have been mapped into the objects' states and covariances by the orbit determination and prediction process. There is no source of future variation or randomness associated with this prediction; the predictions are statistics describing the outcome of the past tracking procedure.* Evidently, under the set of assumptions and models that operators currently employ, and within the context of their operational usage, integrals like Eq. (33) or Eq. (41) cannot be interpreted as relative frequencies associated with possible outcomes of future events, i.e. probabilities.† Instead, they can only be interpreted as statistics, of the same sort as the estimate of the mean and associated covariance.

In many cases, operators can take action to mitigate the risk of a close approach. Since the cost of such action is typically non-trivial, operators have a strong incentive to avoid false alarms. A common practice is to compare P_c to a threshold, and only consider risk mitigation if the threshold is exceeded. This procedure can be rationalized in terms of a Wald test,¹⁸ if one is willing to impose assumptions concerning the prior distributions.

As an alternative, prior to the collection of any tracking data, an analyst may study probabilities of the form¹⁹

$$\gamma = \Pr \left(\vec{\mu}_{\vec{R}} \in \omega(\vec{R}_1, \vec{R}_2, \dots, \vec{R}_n) \right) \quad (51)$$

where $\{\vec{R}_1, \vec{R}_2, \dots, \vec{R}_n\}$ is a random sequence of the relative position vectors, which are to be drawn from a distribution with known covariances[‡] P_1, P_2, \dots, P_n and unknown mean $\vec{\mu}_{\vec{R}}$, corresponding to the true miss vector at the time of closest approach. Realizations of these random vectors will arise from from predictions of the states of the two objects from the times t_1, t_2, \dots, t_n prior to the time of closest approach.

One choice for $\omega(\vec{R}_1, \vec{R}_2, \dots, \vec{R}_n)$ might be an error ellipsoid derived from P_n , centered on a random variable $\hat{\vec{R}}_n$, corresponding to the as-yet-unrealized estimate of the state at t_n . The error

*If the tracking procedure could be repeated, a different set of realizations of the tracking errors would ensue, and a different estimate would derive. In the proverbial long run, over many such repetitions, the estimates could be expected to show a variation about the true state that is consistent with the statistics. This is known as a *Frequentist* viewpoint.

†Under a different set of assumptions, such as including the assumption of prior distributions for the states, and/or the inclusion of stochastic variability (process noise) in the orbit determination and prediction process, it would be meaningful to associate uncertainty with estimates of the object's future states, and the attribution of probability to P_c would remain valid, although probability in this sense is no longer interpretable as a relative frequency. This is known as a *Bayesian* viewpoint.

‡The known covariances can be viewed as being derived without regard for the realized tracking data from a *covariance analysis*.

ellipsoid could be scaled by finding the limits of its corresponding CDF (Eqs. (32) or (41)) that to correspond to a probability of $1 - \alpha$ that $\vec{\mu}_{\hat{R}}$ is contained within it, e.g. using tables of the χ^2 distribution. Then, once an operator has computed a corresponding estimate \hat{r}_n from realizations of the tracking data, she could center the ellipsoid on \hat{r}_n to define a non-point, or *interval* estimate (IE), in this case an ellipsoidal interval estimate. Unlike simply reporting a point estimate for the miss vector, or P_c , which convey some sense of risk without any sense of the quality of the process used to compute the point estimate, the operator has now conveyed information about both the risk, conveyed by the magnitude of the miss vector, and the precision of her estimate. Notably, NASA's Conjunction Assessment and Risk Analysis group provides such data as a supplement to P_c in the reports they provide to their users, some commercial off-the-shelf software packages provide such data, and Reference 20 advocates the superiority of such an approach.

A similar option would be to define a linear region associated with the miss distance, without regard for direction, such as

$$\gamma = 1 - \alpha = \Pr \left(\hat{R}_n - r_\alpha \leq \rho \right) \quad (52)$$

where $\hat{R}_n = \|\hat{R}_n\|$, $\rho = \|\vec{\mu}_{\hat{R}}\|$, and r_α is chosen as the limit of Eq. (33), or Eq. (41) along with estimates of velocity and the full position/velocity covariance, that yields $1 - \alpha$ probability. Once the operator computes an estimate, \hat{r}_n , the inequality

$$\hat{r}_n - r_\alpha \leq \rho \quad (53)$$

defines the one-sided $1 - \alpha$ linear interval estimate $[\hat{r}_n - r_\alpha, \infty)$ * However, the one-sided interval loses the information about precision in much the same manner as P_c does. Instead, from the intersection of intervals corresponding to, for example, $\hat{r}_n - r_{\alpha/2} < \rho$ and $\hat{r}_n + r_{\alpha/2} > \rho$, the operator could compute and report the two-sided $1 - \alpha$ linear interval estimate $[\hat{r}_n - r_{\alpha/2}, \hat{r}_n + r_{\alpha/2}]$, regaining information concerning precision of the estimate.

Coverage

Any particular interval estimate either will or will not contain $\vec{\mu}_{\hat{R}}$, so it is not meaningful to think of it probabilistically. Rather, *if* a $1 - \alpha$ fraction of a large collection of such regions would contain $\vec{\mu}_{\hat{R}}$, for any value of $\vec{\mu}_{\hat{R}}$, then it is known as a (Frequentist) confidence region^{19†}, with *coverage* probability of $1 - \alpha$.

So long as the Gaussian assumption of Eqs. (32) or (41) holds, a $1 - \alpha$ ellipsoidal interval estimate clearly possesses the desired coverage property, because the shape of its PDF does not depend on its location. For any value of $\vec{\mu}_{\hat{R}}$, a $1 - \alpha$ fraction of the resulting estimates \hat{r}_n must lie within the $1 - \alpha$ ellipsoid centered on $\vec{\mu}_{\hat{R}}$, and hence the $1 - \alpha$ ellipsoids centered on each such estimate must contain $\vec{\mu}_{\hat{R}}$. In such cases, if for example the operator chooses $\alpha = 0.05$, she might safely report that she has 95% confidence that the true miss vector lies within the scaled error ellipsoid, so long as her audience appreciates that confidence is not probability.

By contrast, the linear interval estimates $[\hat{r}_n - r_\alpha, \infty)$ and $[\hat{r}_n - r_{\alpha/2}, \hat{r}_n + r_{\alpha/2}]$ do not possess the desired coverage property, because the shape of Eq. (39) or (49) does depend on its proximity

*The sequel discusses intervals such as $[0, \hat{r}_n - r_{1-\alpha}]$.

†If the estimate were derived using Bayesian methods, a *credible region* would result, not necessarily corresponding to the confidence region.

to the origin, and hence there will always be some neighborhood surrounding the origin that such intervals exclude. This fact is evident from Eqs. (33) or (41) by setting $r = \epsilon$. One can always find some ϵ sufficiently close to zero that $F_{R_n}(\epsilon | \vec{\mu}, P_n) = \Pr(R_n \leq \epsilon) < \alpha$. Thus, any true distance $\rho < \epsilon$ will never be included in such an interval.

A linear interval estimate that one constrains to include the origin, such as $[0, \hat{r}_n - r_{1-\alpha}]$, will of necessity exclude points at infinity, and in practice will exclude a large neighborhood of safely large true miss distances. Such intervals may be both uninformatively large, and also fail to satisfy the coverage constraint.

Linear interval estimates of the miss distance therefore cannot be viewed as confidence regions. This fact is related to the defect that occurs when computing P_c from a covariance that is sufficiently large in comparison to the HBR; even if that large covariance is centered on the origin, P_c may fail to rise above any given threshold. Thus, for true miss distances that are small in comparison to the HBR, a decision procedure based on either P_c , or linear interval estimates such as have been so far described herein, will have arbitrarily poor missed detection rates, if their associated covariances are large in comparison to the HBR.

The simplest approach to avoiding this issue is to use ellipsoidal IEs, which are free of the coverage defect, and check for overlap with the combined hard-body volume. However, for the large covariances typical of many debris objects, such a procedure may produce false alarm rates significantly higher than a procedure based on P_c , since overlap between the hard-body volume and any given $k\sigma$ ellipsoid can have arbitrarily small P_c value, well below operationally sustainable P_c thresholds in current usage.

If one wishes to retain a linear interval, then keeping in mind that the coverage property applies to a large collection of estimates with a given covariance, e.g. P_i , and not the sequence of covariances $P_i, i = 1, 2, \dots$, one can adapt the two-sided interval estimate according the covariance as follows. Define the two-sided linear interval estimate $[\hat{r}_n - r_{\alpha_{10}}, \hat{r}_n + r_{\alpha_{hi}}]$ according to

$$\alpha_{hi} = 1 - \alpha + \alpha_{10} \quad (54)$$

$$\alpha_{10} = \min(\alpha/2, \alpha_{0i}) \quad (55)$$

with

$$\alpha_{0i} = F_{R_i}(r_{HBR} | \vec{r}_{0\max}, P_i) \quad (56)$$

where $\vec{r}_{0\max}$ is the miss vector furthest from the origin that would be observed with $1 - \alpha$ confidence if the true miss vector were exactly zero. Such an observation will be on the $1 - \alpha$ iso-probability ellipsoid, along the direction of the eigenvector of P_i corresponding to its maximum eigenvalue. Note that defining the interval in this way depends only the covariance, and not the particular realization of the estimate. Thus, a large collection of such estimates will share consistently-defined limits of their intervals.

Although defining the interval in this manner does not rectify the coverage defect of the linear interval estimates, it ensures that the neighborhood they exclude around the the origin is smaller than r_{HBR} . Thus, for any true miss vector inside the HBR, a $1 - \alpha$ fraction of a large collection of estimates will result in linear interval estimates whose left endpoint penetrates the HBR. A corresponding decision to maneuver in such cases will ensure that the decision procedure has the desired missed detection properties.

Miss Distance Interval Estimate Example

Figure 2 shows an example of the results of a IE calculation for a hypothetical conjunction satisfying the short encounter assumptions. The choice of $\alpha = .05$ and $r_{HBR} = 0.07$ are chosen for clarity of presentation, and not necessarily recommended or typical of conjunction assessment operations. The units are unimportant for this hypothetical case, but one may take them as kilometers for the sake of specificity and/or context.

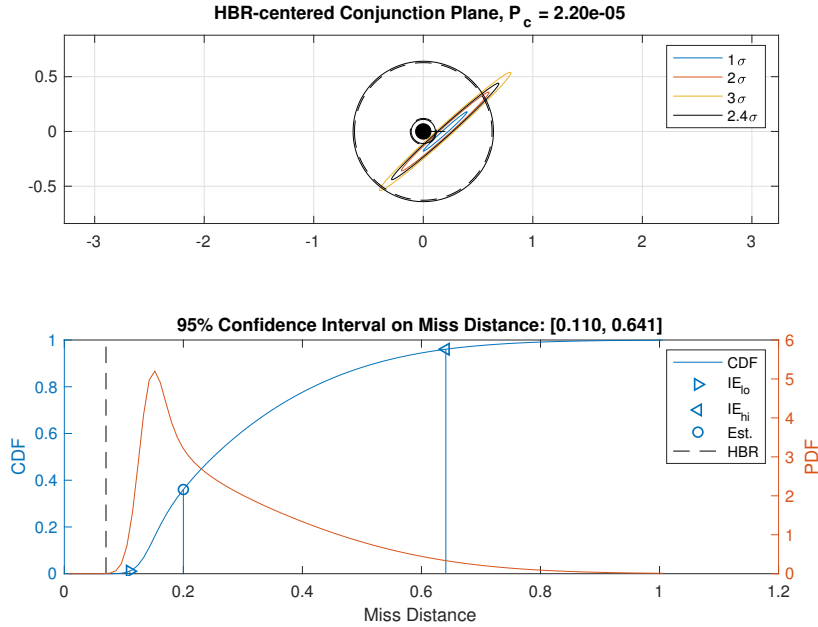


Figure 2: Miss Distance Interval Estimates for a Hypothetical Conjunction.

The upper subplot shows the conjunction plane, and indicates the value of P_c . The colored elliptical contours are centered at the estimated miss vector, and indicate elliptical interval estimates in terms of standard deviation, σ , specified by the legend. The contour labeled 2.4σ corresponds to the $1 - \alpha = 95\%$ elliptical interval estimate. In this view, the 95% linear IE on the miss distance is the (mostly empty) region between the thresholds indicated by the dashed/solid circular boundaries. This conjunction plane view illustrates how the linear IE is less precise than the elliptical IE, since it does not account for the direction of the estimated miss vector. Nonetheless, the linear IE is clearly more robust than the elliptical IE to small variations in the orientation of the ellipses.

The lower subplot shows the CDF for the miss distance, computed from Eq. (33), as a blue line using the left-hand ordinate. The miss distances associated with the HBR, the lower linear IE (IE_{lo}), the upper linear IE (IE_{hi}), and the estimated miss distance (Est.) are all noted by the legend. For this example, the coverage adjustment procedure described above shifted the linear IE toward the origin somewhat, yielding $\alpha_{lo} = 1.05\%$, and hence $\alpha_{hi} = 96.05\%$. The lower subplot also depicts the PDF for the miss distance, computed from Eq. (33), as a red line, using the right-hand ordinate. The PDF clearly shows that \hat{r}_n is not necessarily a maximum likelihood estimate of the miss distance. It is also notable how the miss distance probability mass piles up on the left due to the truncation of the PDF at the origin. Figure 3 illustrates the sensitivity of the PDF to distance of the mean

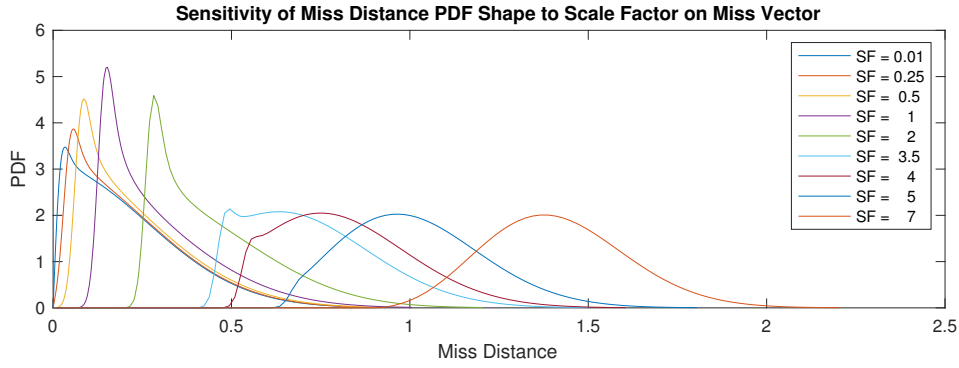


Figure 3: Sensitivity of PDF to Mean for Example shown in Figure 2.

$\rho = \|\vec{\mu}_R\|$ from the origin, which exhibits a notable bimodal aspect during the transition from near-normal appearance at large mean miss distances, to a more and more truncated left-hand tail as the mean nears the origin. Clearly, point estimates such as the estimated mean or maximum likelihood estimate do not tell the full story, except when the miss distance is uninterestingly large.

Figure 4 illustrates an application of the methods advocated herein to a hypothetical close approach. The upper two subplots show the time evolution of 99.98% linear interval estimates of the miss distance, and the associated point miss distance estimate using the left-hand ordinate, with P_c indicated by the right-hand ordinate. Here, α for the interval has been chosen such that $\alpha/2$ would correspond with the an alarm based on a P_c threshold of 1×10^{-4} . The difference between the upper and middle subplots is that the middle subplot illustrates the linear intervals that would result if α_{10} were held fixed at $\alpha/2$. The lower subplot shows the time evolution of elliptical interval estimates (confidence regions) in the HBR-centered conjunction plane corresponding to the same α , which equate to 4.13σ ellipses.

It is notable that early in the encounter, when P_c indicates only moderate risk, both the linear and elliptical interval estimates span many kilometers. This is a direct indication of the lack of precision in these early estimates that P_c alone fails to convey. Also evident is the phenomenon known as “roll-off” of P_c that ensues as the uncertainty shrinks and moves, indicating a “dilution” of P_c early in the encounter.²¹ The use of either linear or elliptical interval estimates objectively conveys this information without the need for such concepts.

Also notable is the manner in which the elliptical CR fully enclose the HBR (which is a barely discernible black speck at the origin, at the scale of the plot) throughout much of the encounter. The linear interval in the upper subplot, which varies α_{10} depending on the covariance, correspondingly includes a region inside the HBR whenever the CR overlaps the HBR.

By contrast, the linear interval based on fixed limits (middle subplot) always leaves some space near the origin, only crossing the HBR when P_c passes a corresponding threshold. Thus, linear intervals with α_{10} held fixed, e.g. at $\alpha/2$, provide an equivalent, but more informative metric to methods based solely on P_c . And the failure of such an interval to cover a neighborhood near the origin is no worse a defect than use of P_c alone entails. Balch, et al.²⁰ provides a related argument against use of P_c in this manner.

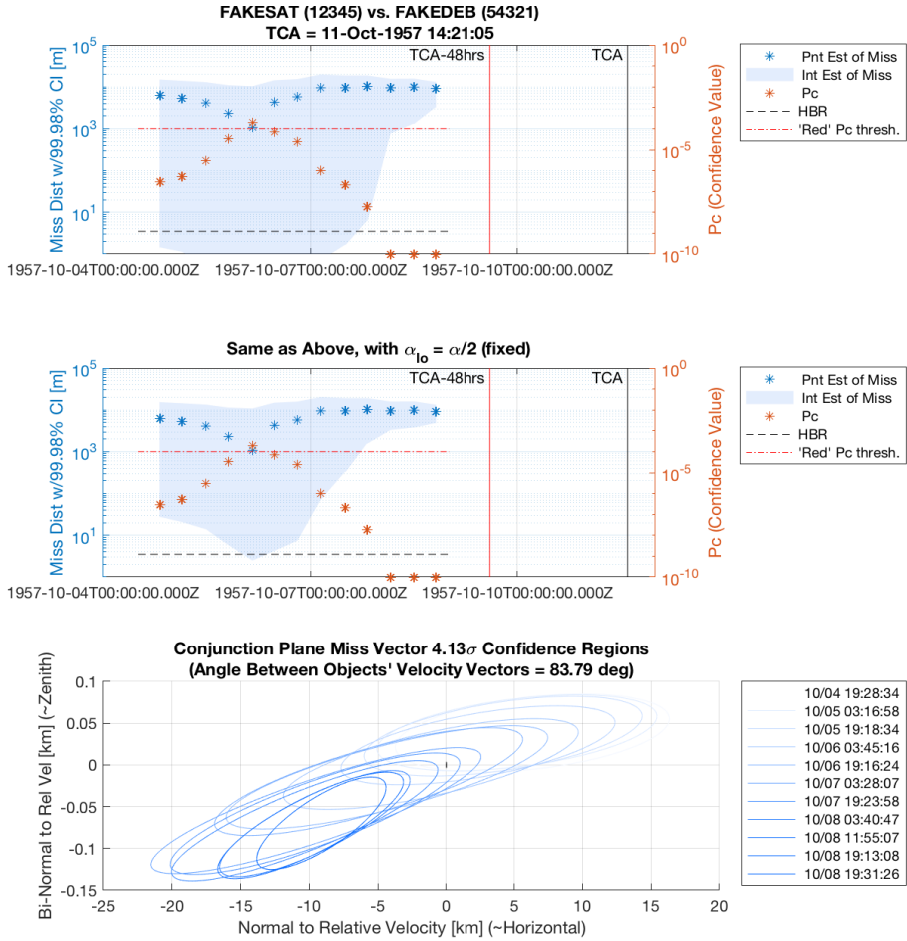


Figure 4: Miss Distance Interval Estimates Time Series.

SUMMARY AND CONCLUSIONS

This paper has described how CDMs could be reformed to avoid the dissemination of NPD covariances, and how cross-covariances between the primary and secondary objects could be relatively easily computed when common *a priori* assumptions in the OD process are present, such as when common ballistic states are included in solving for both vehicles' orbits.

This paper has also described how estimate fusion may be profitably employed to enhance the specificity of conjunction assessments, when multiple sources for state estimates for one or both objects are available. The computations required for fusion also yield information on the consistency of the state estimates, which may be used to quantitatively inflate their covariances to regain consistency. Fusion of relative state information allows for simple synchronization of mildly asynchronous conjunction data, and the consequent need for a cross-covariance is trivially achieved from data already available.

This paper has also described miss distance interval estimates and indicated how two-sided interval estimates may be used in conjunction assessment operations as a more informative metric than

P_c . Linear interval estimates are also evidently more robust to small variations in the conjunction geometry than elliptical interval estimates.

By comparing the lower limit of a linear IE to the HBR, identical decisions to those based on comparing P_c to a threshold would be reached, with judicious choice of a fixed lower limit for the interval. Unlike elliptical intervals, linear interval estimates with fixed lower limits cannot be guaranteed to cover the region inside the HBR for any given covariance, which could result in missed detections if the true miss distance is smaller than the HBR. Comparing a fixed lower limit of a linear IE to the HBR is nonetheless no worse in terms of missed detection rates than comparing P_c to a fixed threshold. With either approach, if there are good reasons to believe that the probability of the true miss vector occurring within the HBR is suitably low, then a “high” missed detection rate does not necessarily lead to the expectation of *any* actual missed detections over timeframes of interest to CA operations.

By choosing a lower threshold that varies with the covariance, the linear interval estimate coverage defect around the origin can be substantially, although not completely mitigated. Doing so results in coverage properties approaching those of elliptical CR, and for practical purposes they are effectively equivalent. Comparing the lower limit of a linear IE that varies with the covariance to the HBR is comparable to comparing P_c to a threshold that similarly varies according to the covariance. Either approach should produce false alarm rates approaching that of checking elliptical CR for overlap with the HBR. Such false alarm rates would be expected to be higher than comparing P_c to a fixed threshold for covariances typical of current operational scenarios.

In conclusion, the CA community faces a dilemma. Current operational procedures do not always produce realistic covariances, and in any case, they are often so “large” that a truly unsafe conjunction could not be reliably detected, as Reference 20 discusses. Changes in procedure to address missed detection concerns, and/or enhancements to covariance realism that do not increase the precision of the estimates, appear likely to drive false alarm rates ever higher. While this paper has offered a few suggestions that could be effectively employed to produce covariances that are both realistic and “smaller,” it remains clear that a substantial improvement in tracking performance is required.

REFERENCES

- [1] A. B. Poore, J. M. Aristoff, J. T. Horwood, R. Armellin, W. T. Cerven, Y. Cheng, C. M. Cox, R. S. Erwin, J. H. Frisbee, M. D. Hejduk, B. A. Jones, P. Di Lizia, D. J. Scheeres, D. A. Vallado, and R. M. Weisman, “Covariance and Uncertainty Realism in Space Surveillance and Tracking,” Accession Number AD1020892, Air Force Space Command Astrodynamics Innovation Committee Working Group on Covariance Realism, Defense Technical Information Center, June 2016.
- [2] J. R. Carpenter, S. Alfano, D. T. Hall, M. D. Hejduk, J. A. Gaebler, M. K. Jah, S. O. Hasan, R. L. Besser, R. R. DeHart, M. G. Duncan, M. S. Herron, and W. J. Guit, “Relevance of the American Statistical Association’s Warning on p -Values for Conjunction Assessment,” *Astrodynamics 2017* (J. S. Parker, J. H. Seago, N. J. Strange, and D. J. Scheeres, eds.), Vol. 162 of *Advances in the Astronautical Sciences*, pp. 921–939, P.O. Box 28130, San Diego, California 92198: Univelt, Incorporated, 2017.
- [3] C. Secretariat, “Conjunction Data Message,” Blue Book CCSDS 508.0-B-1, Consultative Committee for Space Data Systems, Space Communications and Navigation Office, 7L70, Space Operations Mission Directorate, NASA Headquarters, Washington, DC 20546-0001, June 2013.
- [4] J. R. Carpenter and C. N. D’Souza, eds., *Navigation Filter Best Practices*. No. NASA/TP–2018–219822 in NASA Technical Publications (<https://ntrs.nasa.gov>), Washington, DC 20546-0001: National Aeronautics and Space Administration, 1st ed., 2018.
- [5] S. S. Blackman and Y. Bar-Shalom, “Association and Fusion of Multiple Sensor Data,” *Multitarget-Multisensor Tracking: Advanced Applications*, pp. 187–198, Norwood, MA: Artech House, Inc., 1990.

- [6] Y. Bar-Shalom and T. E. Fortmann, "Multisensor Track-to-Track Fusion," *Tracking and Data Association*, pp. 266–272, Academic Press, 1988.
- [7] Y. Bar-Shalom and L. Campo, "The Effect of Common Process Noise on the Two-Sensor Fused-Track Covariance," *IEEE Transactions on Aerospace and Electronic Systems*, Vol. AES–22, No. 6, 1986, pp. 803–805.
- [8] Y. Bar-Shalom, "On the Track-to-Track Correlation Problem," *IEEE Transactions on Automatic Control*, Vol. AC–26, No. 2, 1981, pp. 571–572.
- [9] J. R. Carpenter and R. H. Bishop, "Navigation Filter Estimate Fusion for Enhanced Spacecraft Rendezvous," *Journal of Guidance, Control, and Dynamics*, Vol. 20, March–April 1997, pp. 338–345. also AIAA Paper 94–3548, Aug. 1994, doi.org/10.2514/2.4043.
- [10] J. J. Julier and J. K. Uhlmann, "A Non-Divergent Estimation Algorithm in the Presence of Unknown Correlations," *Proceedings of the American Control Conference*, June 1997, pp. 2369–2373.
- [11] J. L. Foster, Jr. and H. S. Estes, "A Parametric Analysis of Orbital Debris Collision Probability and Maneuver Rate for Space Vehicles," Tech. Rep. JSC–25898, NASA Johnson Space Center, Houston, TX, 1992.
- [12] M. R. Akella and K. T. Alfriend, "Probability of Collision Between Space Objects," *Journal of Guidance, Control, and Dynamics*, Vol. 23, No. 5, 2000, pp. 769–772. doi: 10.2514/2.4611, 10.2514/2.4611.
- [13] V. T. Coppola, "Including Velocity Uncertainty in the Probability of Collision Between Space Objects," *Space Flight Mechanics 2012*, Vol. 143 of *Advances in the Astronautical Sciences*, pp. 2159–2178, Univelt, 2012.
- [14] K. J. DeMars, Y. Cheng, and M. K. Jah, "Collision Probability with Gaussian Mixture Orbit Uncertainty," *Journal of Guidance, Control, and Dynamics*, Vol. 37, No. 3, 2014, pp. 979–985. doi: 10.2514/1.62308, 10.2514/1.62308.
- [15] J. R. Carpenter and R. H. Bishop, "Estimate Fusion for Lunar Rendezvous," *Proceedings of the Guidance, Navigation, and Control Conference*, Washington, DC, AIAA, 1993, pp. 1–10, <https://doi.org/10.2514/6.1993-3700>.
- [16] K. T. Alfriend, M. R. Akella, J. Frisbee, J. L. Foster, Jr., D.-J. Lee, and M. Wilkens, "Probability of Collision Error Analysis," *Space Debris*, Vol. 1, No. 1, 1999, pp. 21–35.
- [17] S. Alfano, "A Numerical Implementation of Spherical Object Collision Probability," *Journal of the Astronautical Sciences*, Vol. 53, Jan–Mar 2005, pp. 103–109.
- [18] J. R. Carpenter and F. L. Markley, "Wald Sequential Probability Ratio Test for Space Object Conjunction Assessment," *Journal of Guidance, Control, and Dynamics*, Vol. 37, 2014/07/15 2014, pp. 1385–1396, 10.2514/1.G000478.
- [19] M. H. DeGroot, *Probability and Statistics*. Addison–Wesley, 1975.
- [20] M. S. Balch, R. Martin, and S. Ferson, "Satellite conjunction analysis and the false confidence theorem," *Proceedings of the Royal Society A*, Vol. 475, 2019.
- [21] S. Alfano, "Relating Position Uncertainty to Maximum Conjunction Probability," *Astrodynamics 2003*, Vol. 116 of *Advances in the Astronautical Sciences*, Univelt, 2004, 10.1.1.372.8578.